Bacterial quorum sensing allows graded and bimodal cellular responses to variations in population density

Jennifer B. Rattray[1,2], Stephen A. Thomas[1,2,3], Yifei Wang[1,2,4], Evgeniya Molotkova[1], James Gurney[1,2], John J. Varga[1,2], Sam P. Brown[1,2]

[1] School of Biological Sciences, Georgia Institute of Technology, Atlanta, 30332 GA, USA
[2] Center for Microbial Dynamics and Infection, Georgia Institute of Technology, Atlanta, 30332 GA, USA
[3] Graduate Program in Quantitative Biosciences (QBioS), Georgia Institute of Technology, Atlanta, 30332 GA, USA
[4] The Institute for Data Engineering and Science (IDEaS), Georgia Institute of Technology, Atlanta, 30332 GA, USA

Corresponding author: Sam P. Brown

Email: sam.brown@biology.gatech.edu

ORCIDs. Jennifer B. Rattray https://orcid.org/0000-0003-3478-2242; Stephen A. Thomas http://orcid.org/0000-0003-0773-0236; Yifei Wang http://orcid.org/0000-0002-7510-7959, James Gurney http://orcid.org/0000-0002-8364-3380, John J. Varga https://orcid.org/0000-0002-4868-1971

Keywords

Bacterial communication, quorum sensing, sociomicrobiology, reaction norm

Author Contributions

J.B.R and S.P.B. conceived the idea and designed the experiment; J.B.R., E.M., J.G., and J.J.V. performed the experiments; J.B.R analyzed the data; and J.B.R., S.A.T, Y.W., J.G., J.J.V., and S.P.B. wrote the paper.

Abstract

Quorum sensing (QS) is a mechanism of cell–cell communication that connects gene expression to environmental conditions (e.g. density) in many bacterial species, mediated by diffusible signal molecules. Current functional studies focus on a dichotomy of QS on/off (or, quorate / sub-quorate) states, overlooking the potential for intermediate, graded responses to shifts in the environment. Here, we track QS regulated protease (*lasB*) expression and show that *Pseudomonas aeruginosa* can deliver a graded behavioral response to fine-scale variation in population density, on both the population and single-cell scales. On the population scale, we see a graded response to variation in environmental population density. On the single-cell scale, we see significant bimodality at higher densities, with separate OFF and ON sub-populations that respond differentially to changes in density; static OFF cells and increasing intensity of expression among ON cells. Together these results indicate that QS can tune gene expression to graded environmental change, with no critical cell mass or 'quorum' at which behavioral responses are activated on either the individual cell or population scale. In an infection context, our results indicate there is not a hard threshold separating sub-quorate 'stealth' mode and a quorate 'attack' mode.

Main Text

Introduction

Many species of bacteria are capable of a form of cell-cell communication via diffusible signal molecules, generally referred to as quorum sensing (QS). The study of QS has largely focused on the intracellular gene regulatory scale, leading to a detailed understanding of the regulatory mechanisms shaping the production of and response to signal molecules in model organisms such as *Vibrio cholerae*, *Bacillus cereus* and *Pseudomonas aeruginosa* [1–3]. We now understand that QS is mediated by multiple diffusible signals that together control a diverse array of responses, including swarming, luminescence, competence and the production of diverse secreted factors [4,5]

While the molecular mechanisms of QS have been described for model organisms in remarkable detail, the functional and evolutionary context of QS continues to be disputed. In other words, while we now have a better understanding of *how* QS works, we still have limited understanding of *why* bacteria use this system to control behavior. What are the functions of QS? How do these QS functions help bacteria to survive and grow? The standard answer is that bacteria use QS to sense when they are at sufficient density ('quorate') to efficiently turn on cooperative behaviors such as secretion of toxins and enzymes in order to collectively modify their environment [6].

Other researchers have argued that QS is an asocial sensing apparatus, where individual cells produce and monitor signal levels in order to infer their physical environment (am I in an open or enclosed space?) [7]. More recently, integration of molecular and evolutionary approaches has increased the menu of potential functions to include sensing multiple aspects of both the social and physical environment [6,8–10] and coordinating complex social strategies that limit the profitability of non-cooperating 'cheat' strains [11–18].

A critical step in assessing the various adaptive hypotheses is establishing the functional capacities and limits of QS. Previous studies have demonstrated 'density sensing' functions – populations can use QS to sense when they exceed a density threshold [6,19,20]. In addition, Darch et al. (2012) demonstrated that responding with increased QS controlled cooperative activity at high density can provide a fitness benefit [6]. Other studies have demonstrated 'diffusion sensing' functions [7] – QS systems can functionally respond to variation in physical containment, so that even a single cell can become 'quorate' (turn on a QS controlled reporter gene) if isolated in a sufficiently small contained space [9]. More recently, some studies have demonstrated 'genotype sensing' functions – QS can respond to variation in the genotypic composition of a population, restricting QS-controlled responses to populations that are enriched with wildtypes [11,14,21,22].

The functional studies outlined above largely focus on a dichotomy of QS on/off (or, quorate / sub-quorate) states, overlooking the potential for intermediate, graded responses (Fig 1A). The threshold quorate/non-quorate concept is ingrained in the QS literature following the use of the legal 'quorum' analogy [20], and is also supported by mathematical models of QS signal dynamics that highlight how sufficiently strong positive feedback control of signal production can produce a sharp threshold response to changes in environmental parameters such as density or diffusion [23,24]. However, these same mathematical models indicate that graded responses are also possible, dependent on the model parameterization. More generally, Fig 1A highlights that the phenotypic response of QS bacteria to differing environmental conditions can be viewed as a 'reaction norm' [25–28] that can in principle take differing shapes. Reaction norms describe phenotypic responses of a single genotype (y-axis, Fig 1A) to varying environmental inputs (x-axis, Fig 1A). Incorporating a reaction norm framework provides a menu of quantitative metrics to define QS responses to environmental variation (e.g., slope, intercept, and variances). With this reaction norm framework, it is important to emphasize that in our study the x-axis is not time, but instead captures a gradient of environmental conditions. Whether responses are graded or thresholded during the growth towards high density is a separate line of inquiry [29]. Describing the reaction-norms of QS cells and populations to contrasting environments is an important step

towards understanding the capacities of QS systems to differentially respond to novel environments.

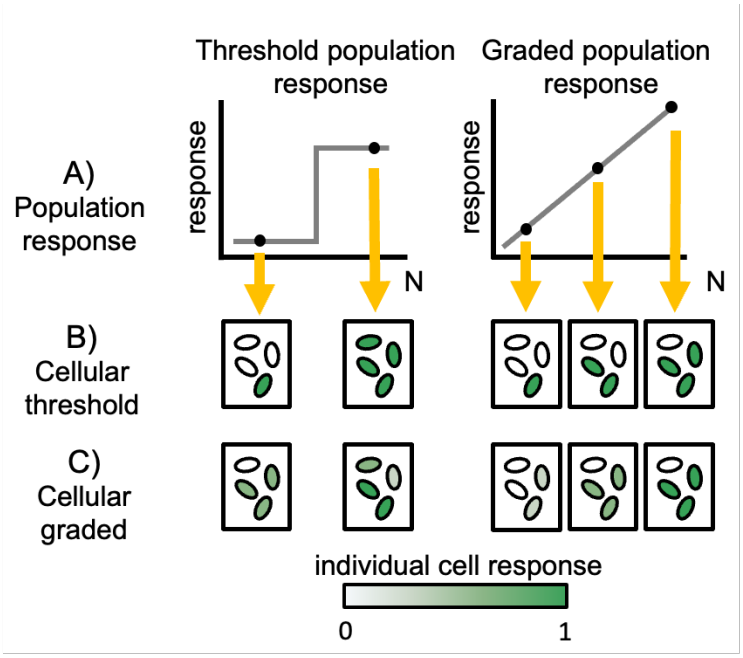

Figure 1. Schematic of potential population and single cell responses to variation in cell density. A) Population response (y-axis) across discrete carrying capacity environments (N, x-axis), given a threshold (left) or graded response (right). In (B) and (C) we outline alternative cell-scale responses (intensity of green cells) that are consistent with discrete population scale behaviors (yellow arrows). (B) threshold (ON/OFF) cellular responses can produce a threshold or graded responses on population scale. (C) graded individual responses can produce threshold or graded responses on a population scale.

Whether the population scale reaction norm to environmental variation is threshold-like or graded (Fig 1A), a separate question is how collective population-level responses are constructed out of individual cellular contributions (Fig 1B,C). Studies of QS on a single-cell scale have revealed substantial heterogeneity in response to QS signals [9,30–36], highlighting that cell-cell communication does not necessarily result in tight synchronization of individual cell activity (Fig 1B,C). In some systems, heterogeneity can be quenched by the addition of extra signal [31,33], implying a lack of receptor saturation. However, this is not a universal result [30], indicating that other molecular processes can drive cellular variation in response. Regardless of the molecular details, we currently lack a behavioral understanding of how individual cellular responses vary with changes in the environment.

In the current study we address the canonical ‘density sensing’ function of QS, using the environmental generalist and opportunistic pathogen *Pseudomonas aeruginosa*, and an unprecedented scale of environmental resolution (13 discrete limiting carbon levels conducted in

triplicate, generating 39 density environments). QS in *Pseudomonas aeruginosa* is heavily studied in a high-density context, revealing a complex mechanism of multi-signal control [37–41]. Our first challenge is to map the population scale resolving power of QS to quantitatively discriminate graded differences in population density (Fig 1A). Does *P. aeruginosa* respond in a purely threshold manner, collapsing quantitative differences in population density into a simple low / high qualitative output, or can QS allow *P. aeruginosa* to deliver a graded response to distinct environmental densities? Our second challenge is to understand how collective responses are partitioned across individual cells. Are changes in collective responses governed primarily by changes in the proportion of cells in an on state (Fig 1B) or changes in the individual cell intensity of response (Fig 1C), or both?

Results

Collective level of response to density is graded and linear. Our first challenge is to map out the population scale reaction norm of the collective QS-controlled protease (*lasB*) response to variation in population densities. To provide a detailed picture of the QS response reaction norm to varying density, we grew a QS reporter strain (PAO1 pMHLAS containing the *PlasB::gfp(ASV)* reporter construct for QS regulated protease expression [42]) under 13 conditions of carbon limitation in triplicate and measured average fluorescence output per cell as the populations reach carrying capacity (Fig 2). Dead cells with compromised membranes were identified with a propidium iodide stain and excluded from analysis. The range of cell densities generated from this method is from $1x10^8$ cells/ml to $2x10^9$ cells/ml. Figure 2 shows that QS response is linear with increasing culture density, providing intermediate levels of average per-capita response to intermediate densities. To confirm the lack of threshold behavior we assessed alternate statistical models including threshold functions, and found that a linear fit model supports the data better than a step-function fit (AIC linear: 89, AIC step-function: 190; relative likelihood that the linear model is the best fit compared to step-function > 10^9, see [43]), supporting a graded population response as outlined in Figure 1. This agrees with literature that QS induction at lower population densities is possible [6,9,19], but differs in that there is no observable population density at which populations ‘switch’, or reach quorum, into a responsive state.

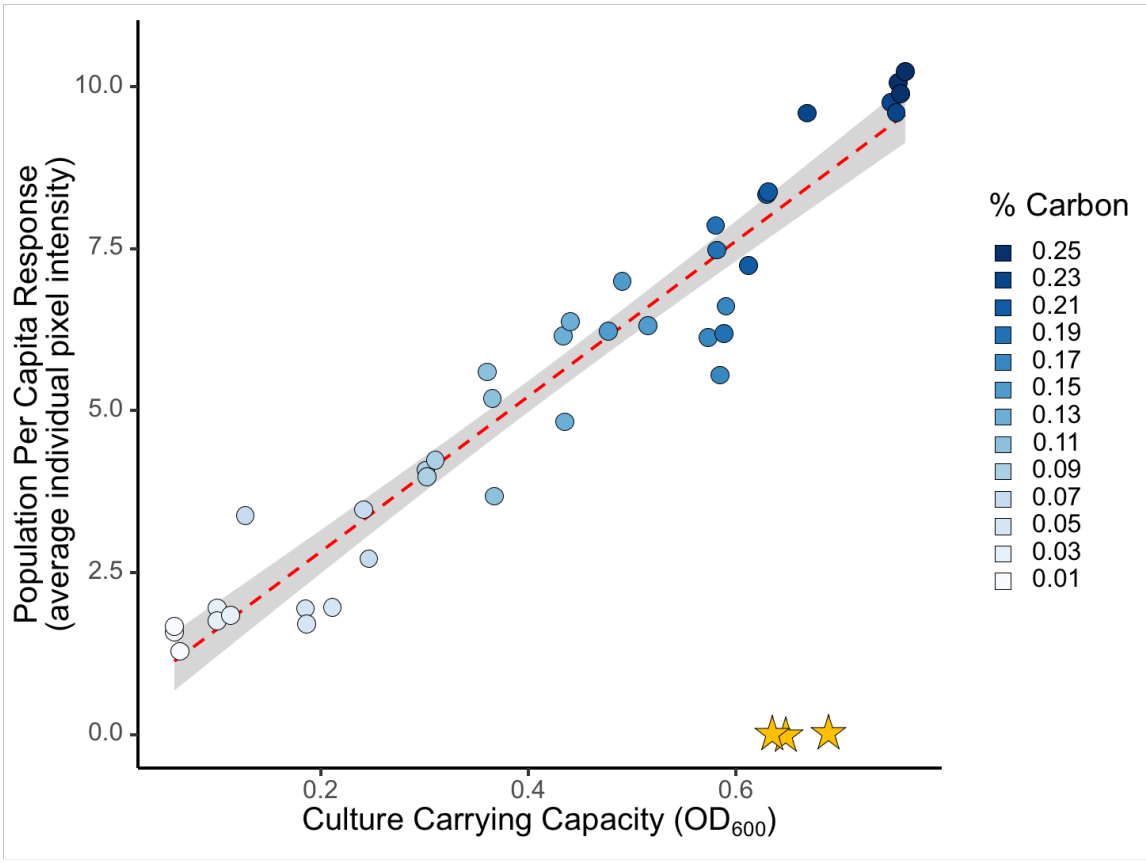

Figure 2. Population response to increasing cell density is linear and graded. 13 distinct culture carrying capacities were generated by manipulating the concentration of casein digest as the limiting resource (Fig S1). Cells were grown to carrying capacity in triplicate and immediately assayed for QS response via fluorescence microscopy imaging. Response is determined by a fusion of the quorum sensing controlled *lasB* promoter and an unstable green fluorescent protein (PAO1 pMHLAS containing *PlasB::gfp(ASV)*). Individual cell pixel intensity is a measure of cellular quorum sensing response and average pixel intensity is calculated across all cells in the population as a proxy for total population expression. Microscopy averages are congruent with population scale plate reader results (Figure S2). A quorum sensing signal knockout (Δ*lasI*Δ*rhlI*), yellow star, shows background response with no signal in the environment. Average population investment in QS increases as culture density increases with no observable density threshold (AIC linear: 89, AIC step-function: 190).

Individual response to density is bimodal at high densities. Figure 2 establishes that on a collective population scale, the response to environmental variation (in density) is smoothly graded. Next, we ask how this collective response is built from individual cell contributions. Is the graded increase due to more cells turning on at higher densities (Figure 1B), cells turning on to a greater extent (Figure 1C), or both? To address this question, we take the same data presented

143 in Figure 2 and now present the distribution of individual cellular responses rather than simply the
144 mean response (Figure 3).
145

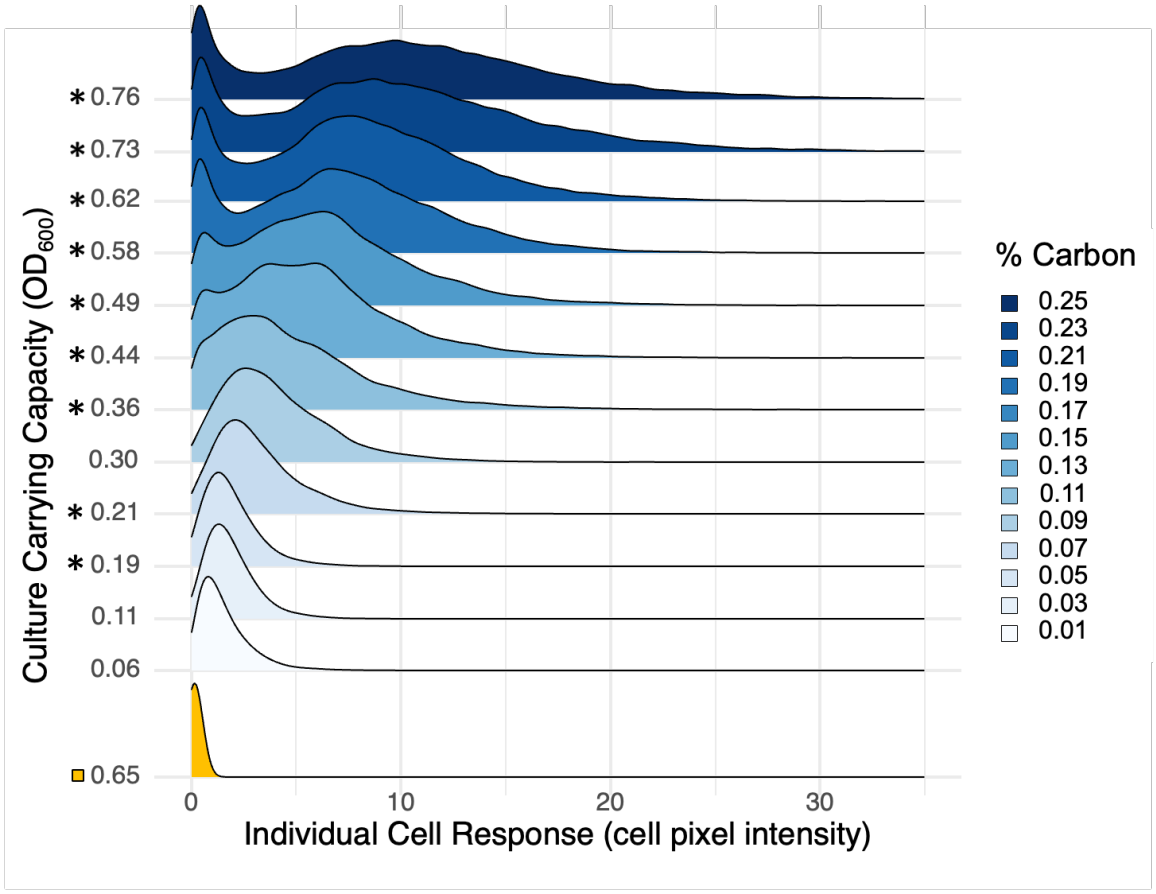

146
147 **Figure 3. Individual response is heterogenous and bimodal at higher densities.** Ridgeline density plot
148 (bandwidth = 0.435) of single-cell *lasB* reporter response data showing the distribution of individual cell QS
149 expression across the population. For brevity and plotting purposes, carrying capacities were averaged
150 across 3 replicates for each of the 13 carbon environments before plotting. A full plot of each independent
151 replicate environment can be found in Figure S3. Each line summarizes 18,000 to 30,000 individual cell
152 measurements, scaled to a unit height. Asterisks indicate significant bimodality (Hartingan's Dip Test [44],
153 Figure S4). The quorum sensing signal knockout (*ΔlasIΔrhlI*) is denoted with yellow boxes. A total of
154 345,000 individual cell measurements were analyzed.
155
156 As expected from prior studies in other QS systems [9,30–36], plotting all individual responses
157 within a population shows cell-to-cell variation in QS response within a single population despite
158 isogenic and homogenous culture conditions (Figure 3). In addition, at higher densities we see
159 significant bimodality (defined by Hartigan's Dip Test, Figure S4), with the population segregating
160 into an unresponsive, sub-quorate, OFF state and a responsive, quorate, ON state.
161

In light of this bimodality, we fit a two-component finite mixture model to the data (Figure 4A, see Figures S10-S13 and Table S2 for extended analysis), which allows us to define the average intensity of the ON state (Figure 4B) and the proportion of cells in the OFF or ON states (Figure 4C).

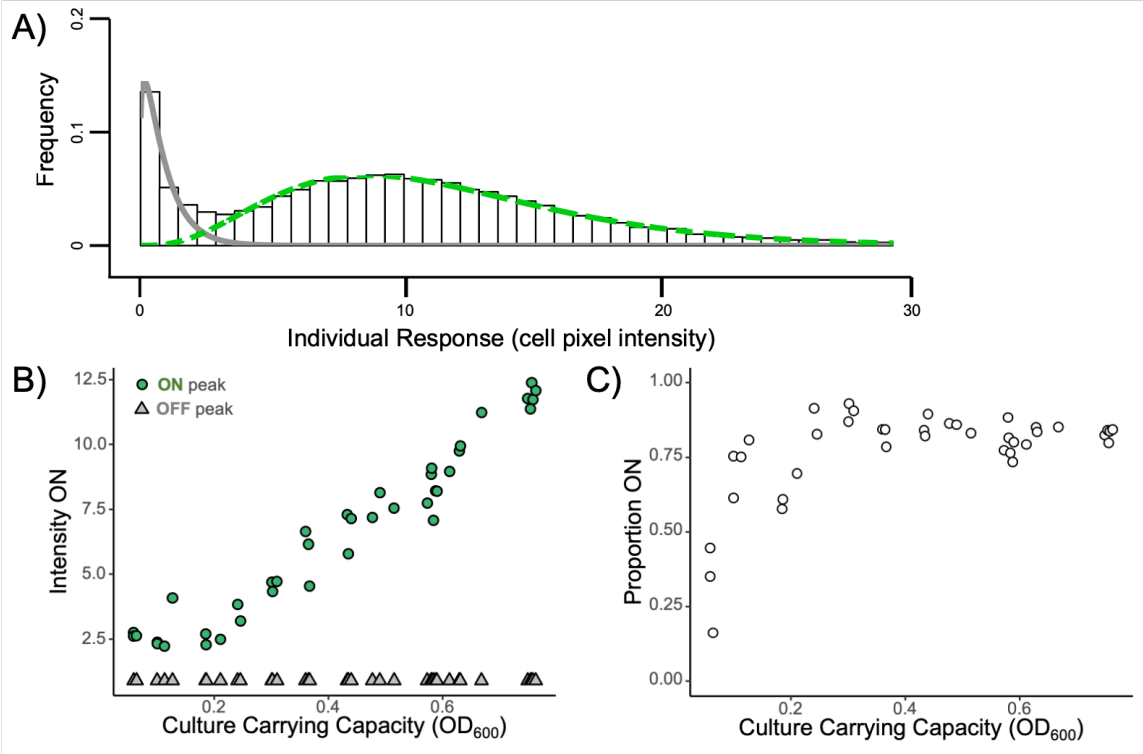

Figure 4. Proportion of cells responding and level of response varies with density. In light of the bimodal responses in Figure 3, we course-grain the single-cell *lasB* response data into discrete ON/OFF states. A) Method summary. We quantify distinct ON/OFF states by fitting a two-component finite mixture model at each measured optical density, where the OFF state is fixed to the OFF state of the highest density environment. The histogram shows the distribution of cellular expression levels at a single density treatment (0.76 OD_{600}), the grey line is the fitted OFF state and the green dashed line is the fitted ON state. B) The mean intensity of the ON (green circle) and OFF (grey triangle) states is determined from the means of mixture model component fits (green and grey lines in panel A). The mean intensity of the ON state distribution increases as culture density increases, while the mean of the OFF state remains constant. C) The proportion of cells ON in the population is determined from the relative mass of cells in the model component fits. The proportion ON increases with culture density but does not reach 100%.

Figure 4B illustrates a graded linear increase in the intensity of the ON state with increasing environmental density, and a density-invariant off state. Figure 4C illustrates that the proportion of cells that are ON plateaus at around 85% at densities with consistent support for bimodality (above 0.36 OD_{600}). At lower densities, the intensity of the ON state (Figure 4B) declines to a point where the OFF and ON states are no longer significantly different and the dip test fails to reject uni-modality (Figure S4). In supplemental materials, we present alternate statistical

analyses of this data, and of other related datasets. Across other experiments, we find consistent support for the graded and bimodal response pattern on the single-cell scale across multiple assay time-points (Figure S5) and across two reporter strain constructs (Figure S6) and support for the graded and linear response pattern on the population scale across fluorescent and lux reporters (Figure S2, Figure S7). We find further support for the graded reaction norm on the population scale across two additional QS controlled genes (*pqsA, rhlI;* Figure S7).

Discussion

Our results show that populations of *P. aeruginosa* can respond in a smoothly graded manner to variation in environmental density (Figure 2), that populations exhibit significant bimodality at higher densities (Figure 3), and that this population scale graded response can be described by the number of responsive 'ON' cells and the intensity of the 'ON' state (Figure 4). The ability to achieve a graded population scale response implies in principle that *P. aeruginosa* can tune collective responses (such as the secreted elastase virulence factor produced by our *lasB* reporter gene) to graded environmental changes, rather than simply course-graining into a simple 'high / low' dichotomy. A similar population scale graded response to continuous environmental variation is visible in the data from Allen et al., which looked at variation in the genotypic composition of mixed populations grown to the same total density [11]. As the proportion of wildtype (PAO1 versus Δ*lasR* 'cheats') increased, the wildtype per-capita investment in cooperative LasB secretions also increased, providing a simple behavioral mechanism to protect cooperative investments from exploitation by cheats [11,22].

The existence of graded population scale responses across two continuously varying environmental inputs (density, genotypic composition) raises the question of why use a graded response? Is there an evolutionary rationale for a graded response, or is a graded increase simply the 'best approximation' of a threshold response, given a simple system working under genetic constraints? Existing evolutionary theory suggest that graded investment reaction norms can be adaptive, under a range of distinct scenarios [45,46] (34, 35). In the specific context of quorum-sensing bacteria, evolutionary theory suggests that population scale responses to increasing density should depend critically on the shape of the cost and benefit functions of increasing cooperative investments. Specifically, a graded response is predicted to be the optimal strategy if the benefit function is decelerating and costs are linear with increasing investment [47].

To further consider the functional context of the graded reaction norms, we turn to the single cell scale data, which reveals how the graded population response is built from the contributions of individual cells. In agreement with previous work in multiple quorum-sensing organisms [9,30–36,48,49], we find cell-scale heterogeneity. In addition, our results illustrate how cellular

222 heterogeneity changes with the environment, demonstrating the onset of ON/OFF bimodality at
223 intermediate densities, with both the proportion of cells ON and the intensity of the cellular ON
224 states increasing with increases in culture carrying capacity (Figures 3 & 4).
225
226 The presence of a bimodal QS response is in contrast with the common view of QS as a
227 mechanism of cell synchronization yet can be viewed as a striking example of widely observed
228 cellular heterogeneity under QS control. Indeed, bimodal responses are implicit in some of the
229 previous single-cell QS literature [31,32,49], for example Darch et al. (2018) report distinct
230 populations of QS-responsive and non-responsive cells within single experimental runs [49]. The
231 degree of heterogeneity in any cellular trait can be interpreted as the interplay of biochemical
232 properties of molecules and the architecture of gene-regulatory networks [50]. Given that
233 regulatory networks are subject to mutation and selection, this implies that the degree of
234 heterogeneity is an evolvable trait [51]. In the context of QS, positive feedback loops (signal auto-
235 regulation [52]) and the presence of cooperative transcription factor binding [53] provides
236 recognized regulatory ingredients for bimodal expression [54]. Recently, the presence of
237 heterogeneous QS response at the single-cell scale has been ascribed to a potential bet-hedge
238 against mis-directed QS induction [48], suggesting that our OFF cells are poised to more quickly
239 resume growth in the event of a rapid return to a growth-friendly environment.
240
241 We made a number of specific observational choices in order to conduct our experiment that
242 could have shaped our results in ways that are not generalizable to other contexts. In the
243 supplementary we detail a number of additional experiments (and alternate statistical analysis
244 approaches) that collectively illustrate the robustness of our findings. In brief, we found that our
245 single cell results are not sensitive to the time the population was sampled (Figure S5), the
246 presence of a potentially leaky P*lac::lasR* on the pMHLAS construct (Figure S6), or the plasmid
247 nature of the pMHLAS construct (Figure S6). Additionally, we recognize that *lasB* is only one
248 gene out of hundreds that are controlled by QS [3], and is often co-regulated by other factors [55–
249 57]. We chose to initially focus on *lasB* as it is a traditionally studied QS-controlled trait [58–60], it
250 is under multi-signal control [10,61] and has clinical significance as a virulence factor [62,63]. To
251 begin to address the generality of our results across genes in *P. aeruginosa*, we show that two
252 other QS regulated genes with complex promoters, *pqsA* and *rhlI*, also support a graded
253 population response (Figure S7). It remains to be seen whether the graded responses we report
254 here are consistent across all QS controlled genes in *P. aeruginosa*, and across QS systems in
255 other species,
256
257 A recent transcriptomic analysis of clinical versus *in vitro* gene expression in *P. aeruginosa* called
258 into question the clinical relevance of *in vitro* models of QS, reporting that QS activity (including

259 *lasB* expression) was systematically higher in *in vitro* models [64]. Our results provide a simple
260 interpretation of this difference: *in vitro* models are typically conducted under higher experimental
261 densities, resulting in higher levels of average QS gene expression (Figure 2). Consistent with
262 this graded response interpretation, Cornforth et al. (2018) also reported higher levels of relative
263 expression in *in vitro* biofilm models (close-packed cells, the highest local density achievable)
264 compared to *in vitro* planktonic models.
265
266 In summary, our results provide a finely resolved mapping of the QS reaction norm to
267 environmental density in PAO1, on both the collective and single-cell scale. On the population
268 scale we see a graded linear response across a range of cellular densities ($1x10^8$ cells/ml to
269 $2x10^9$ cells/ml) and significant individual-scale bimodality at higher densities. We further resolve
270 this linear population response (Figure 2) into a combination of the likelihood of being responsive
271 and the intensity of response (Figure 4). In an infection context, our results indicate that there is
272 no hard threshold separating sub-quorate 'stealth' mode and a quorate 'attack' mode [65]. One
273 implication is that attempts to control virulence and biofilm expression in medicine and industry
274 via QS inhibition could have impacts across a wider spectrum of population densities. In this
275 applied context, it is important to assess the generality of our results and ask, how do QS
276 reaction-norms vary across strains and species of QS bacteria? How do they vary across
277 environments? More broadly, our work undermines the threshold concept of a 'quorum', instead
278 placing QS bacteria in the graded world of reaction norms.
279
280
281 **Materials and Methods**
282 **Bacterial Strains and Growth Conditions**. The two main bacterial strains used in this study are
283 *P. aeruginosa* NPAO1 (Nottingham-PAO1) containing the *PlasB::gfp(ASV)* quorum sensing
284 reporter pMHLAS [42] and a double signal synthase mutant incapable of producing QS signal
285 molecules, *P. aeruginosa* NPAO1 *ΔlasI/ΔrhlI* containing the same *PlasB::gfp(ASV)* quorum
286 sensing reporter pMHLAS. A complete table of strains used in the main text and supplemental
287 figures can be found in Supplemental Table 1. Overnight cultures were grown in lysogeny broth
288 (LB), supplemented with 50 ug/ml gentamicin to maintain the pMHLAS plasmid, with shaking at
289 37 °C. Experiments were conducted in lightly buffered (50 mM MOPS) M9 minimal defined media
290 composed of an autoclaved basal salts solution (Na_2HPO_4, 6.8 gL^{-1}; KH_2PO_4, 3.0 gL^{-1}; NaCl, 0.5
291 gL^{-1}), and filter-sterilized 1 mM $MgSO_4$, 100 uM $CaCl_2$, and 1X Hutner's Trace Elements with
292 casein digest, as the sole carbon source (ThermoFisher Difco™ Casein Digest CAT 211610).
293
294 **Controlling Culture Carrying Capacity**. We manipulated density by controlling the limiting
295 resource in the media, carbon, allowing us to tune the carrying capacity of each treatment (Figure

296 S1). To cover a variety of densities, we generated a carbon range between 0.05% and 0.25% via
297 dilutions of a 0.5% carbon minimal media stock for a total of 13 different carrying capacities with
298 three replicates each. This produced a range of densities environments from 1.18×10^8 cells/ml to
299 2.02×10^9 cells/ml. Overnight cultures were grown in LB gentamicin 50 ug/ml and centrifuged at
300 8,500 x g for 2 minutes. The cells were then washed twice with carbonless minimal media and
301 then each carbon treatment was adjusted to OD_{600} = 0.05. Then, 200 uL of each sample was
302 added to a 96-well microplate. Plates were incubated with shaking at 37 °C in a Cytation/BioSpa
303 plate reader and growth curves were generated by absorbance (OD_{600}) readings taken at 30-min
304 intervals.
305
306 **Measuring Population QS Response.** To measure population response, we performed growth-
307 curve experiments as previously described using PAO1 *PlasB::gfp(ASV)*, additionally taking
308 fluorescence readings at 30-min intervals. Fluorescence, population level response, was
309 recorded when populations reached the end of their exponential growth phase, before they
310 entered stationary phase. Background fluorescence of the reporter was determined with the QS
311 signal deficient mutant PAO1 *ΔlasI/ΔrhlI PlasB::gfp(ASV).* The population microplate data (Figure
312 S2) and averaged microscope data (Figure 2) agreed, so the latter is provided in the primary text.
313
314 **Measuring Individual QS Response.** To measure individual response, we performed growth-
315 curve experiments as previously described, but removed samples for microscopy once cells
316 reached end exponential phase. Since we control carrying capacity with the amount of carbon,
317 the exact time that cells reach the end of exponential growth differs across treatments by 2-3
318 hours. To robustly sample cultures at this specific point, the slope of the two most recent time
319 points on the growth curve was monitored and samples were taken as the slope approached 0.
320 Replicate wells were kept growing to confirm that the treatment entered stationary phase right
321 after the sampling time point. We also determined that our results are generalizable even when
322 sampling at a pre-determined hour across concentrations (Figure S5). Samples were stained with
323 propidium iodide to differentiate between life and dead cells and a small aliquot (5 ul) was added
324 to a 0.01% poly-l-lysine coated slide to immobilize cells and immediately imaged to avoid
325 changes in expression between sample acquisition and imaging in the dark on a Nikon Eclipse TI
326 inverted microscope at 20x magnification. Live cell fluorescence microscopy was used for this
327 study as fluorophores can be sensitive to fixation/permeabilization. These techniques can result
328 in a decrease in fluorescence and therefore decrease in the observable dynamic range. Bright
329 field, green fluorescence (20% Lumencor light engine power, 200ms exposure, and 64x gain-
330 sufficient for imaging of low fluorescent cells without saturating pixel intensity), and red
331 fluorescence (20% Lumencor light engine power, 800ms exposure, and 64x gain) channels were
332 captured. Between 5,000 and 15,000 individual cells were captured for each sample. Aliquots

333 were diluted immediately before imaging with carbonless minimal media when required to ensure
334 an even distribution of cells.

335 **Single cell image analysis.** A custom macro in ImageJ was written to analyze the image data,
336 outlined in Figure S8. The macro uses ImageJ's "analyze particles" command to identify single
337 cells on the bright field image. This then generates a ROI (region of interest) for each individual
338 cell and these ROIs were then overlaid onto the corresponding fluorescent image. The red
339 fluorescence channel was used to identify dead cells with compromised membranes, which were
340 excluded from further analysis. The green fluorescence channel reflected the QS reporter and
341 pixel intensity was measured as a proxy for level of QS response. This tabulated live cell
342 expression data was then analyzed using *Stata Statistical Software: Release 17* from StataCorp
343 LLC. In order to improve the fit of the mixed models, the lowest pixel intensity measurement in the
344 highest carbon PAO1 *ΔlasI/ΔrhlI PlasB::gfp(ASV)* treatment was subtracted from all pixel
345 intensities so that expression started at 0.

346 **Statistical analysis summary.** The analysis was done using *Stata Statistical Software: Release*
347 *17* from StataCorp LLC and the additional third party resources: [66–70]. Each of the 39
348 populations was fit to a finite mixture model of two Gamma distributions. The latent classes in the
349 mixture model correspond to OFF and ON cells. Gamma distributions are preferred to Normal
350 distributions as gene expression is strictly non-negative and necessarily right-skewed. The
351 models provide maximum likelihood estimates of the proportion of cells in each latent class and
352 the shape and scale parameters of the component Gamma distributions. Mean expression level
353 for each distribution is the product of shape and scale parameters. Information criteria for
354 aggregate mean expression level was also calculated using Stata.

355 **Acknowledgments**

356 We thank Steve Diggle, Marvin Whitely, Kathleen O'Connor and members of the Center for
357 Microbial Dynamics and Infection (CMDI) for valuable comments and discussion on this work. We
358 thank Dr. Kasper Norskov Kragh for the *PlasB::gfp(ASV)* reporter construct. This research was
359 supported by the National Science Foundation Graduate Research Fellowship Program under
360 Grant No. DGE-1650044, The Simons Foundation Grant No. 396001, and National Institute of
361 Health Grants 1R21AI143296 and 1R21AI156817.

362

363 **References**

364 1. Rutherford ST, Bassler BL. Bacterial quorum sensing: Its role in virulence and possibilities
365 for its control. Cold Spring Harbor Perspectives in Medicine. Cold Spring Harbor
366 Laboratory Press; 2012. doi:10.1101/cshperspect.a012427

2. Abisado RG, Benomar S, Klaus JR, Dandekar AA, Chandler JR. Bacterial Quorum Sensing and Microbial Community Interactions. Garsin DA, editor. MBio. 2018;9: e02331-17. doi:10.1128/mBio.02331-17

3. Whiteley M, Diggle SP, Greenberg EP. Progress in and promise of bacterial quorum sensing research. Nature. Nature Publishing Group; 2017. pp. 313–320. doi:10.1038/nature24624

4. Miller MB, Bassler BL. Quorum Sensing in Bacteria. Annu Rev Microbiol. 2001;55: 165–199. doi:10.1146/annurev.micro.55.1.165

5. Popat R, Cornforth DM, McNally L, Brown SP. Collective sensing and collective responses in quorum-sensing bacteria. J R Soc Interface. 2015;12. doi:10.1098/rsif.2014.0882

6. Darch SE, West SA, Winzer K, Diggle SP. Density-dependent fitness benefits in quorum-sensing bacterial populations. Proc Natl Acad Sci. 2012;109: 8259–8263. doi:10.1073/pnas.1118131109

7. Redfield RJ. Is quorum sensing a side effect of diffusion sensing? Trends Microbiol. 2002;10: 365–70. doi:10.1016/s0966-842x(02)02400-9

8. Hense BA, Kuttler C, Müller J, Rothballer M, Hartmann A, Kreft JU. Does efficiency sensing unify diffusion and quorum sensing? Nat Rev Microbiol. 2007;5: 230–239. doi:10.1038/nrmicro1600

9. Boedicker JQ, Vincent ME, Ismagilov RF. Microfluidic Confinement of Single Cells of Bacteria in Small Volumes Initiates High-Density Behavior of Quorum Sensing and Growth and Reveals Its Variability. Angew Chemie Int Ed. 2009;48: 5908–5911. doi:10.1002/anie.200901550

10. Cornforth DM, Popat R, McNally L, Gurney J, Scott-Phillips TC, Ivens A, et al. Combinatorial quorum sensing allows bacteria to resolve their social and physical environment. Proc Natl Acad Sci U S A. 2014;111: 4280–4284. doi:10.1073/pnas.1319175111

11. Allen RC, McNally L, Popat R, Brown SP. Quorum sensing protects bacterial co-operation from exploitation by cheats. ISME J. 2016;10: 1706–1716. doi:10.1038/ismej.2015.232

12. Eldar A. Social conflict drives the evolutionary divergence of quorum sensing. Proc Natl Acad Sci U S A. 2011;108: 13635–13640. doi:10.1073/pnas.1102923108

13. Smalley NE, An D, Parsek MR, Chandler JR, Dandekar AA. Quorum Sensing Protects Pseudomonas aeruginosa against Cheating by Other Species in a Laboratory Coculture Model. Silhavy TJ, editor. J Bacteriol. 2015;197: 3154 LP – 3159. doi:10.1128/JB.00482-15

14. Even-Tov E, Omer Bendori S, Valastyan J, Ke X, Pollak S, Bareia T, et al. Social Evolution Selects for Redundancy in Bacterial Quorum Sensing. Gore J, editor. PLOS Biol. 2016;14: e1002386. doi:10.1371/journal.pbio.1002386

15. Granato ET, Kümmerli R. The path to re-evolve cooperation is constrained in Pseudomonas aeruginosa. BMC Evol Biol. 2017;17: 214. doi:10.1186/s12862-017-1060-6

16. Özkaya Ö, Balbontín R, Gordo I, Xavier KB. Cheating on Cheaters Stabilizes Cooperation in Pseudomonas aeruginosa. Curr Biol. 2018;28: 2070-2080.e6. doi:10.1016/j.cub.2018.04.093

17. Chen R, Déziel E, Groleau MC, Schaefer AL, Greenberg EP. Social cheating in a

Pseudomonas aeruginosa quorum-sensing variant. Proceedings of the National Academy of Sciences of the United States of America. National Academy of Sciences; 2019. pp. 7021–7026. doi:10.1073/pnas.1819801116

18. Gurney J, Azimi S, Brown SP, Diggle SP. Combinatorial quorum sensing in Pseudomonas aeruginosa allows for novel cheating strategies. Microbiology. 2020; micro000941. doi:10.1099/mic.0.000941

19. Connell JL, Wessel AK, Parsek MR, Ellington AD, Whiteley M, Shear JB. Probing prokaryotic social behaviors with bacterial “lobster traps.” MBio. 2010;1. doi:10.1128/mBio.00202-10

20. Fuqua WC, Winans SC, Greenberg EP. Quorum sensing in bacteria: The LuxR-LuxI family of cell density- responsive transcriptional regulators. Journal of Bacteriology. American Society for Microbiology; 1994. pp. 269–275. doi:10.1128/jb.176.2.269-275.1994

21. Schluter J, Schoech AP, Foster KR, Mitri S. The Evolution of Quorum Sensing as a Mechanism to Infer Kinship. Locke JCW, editor. PLOS Comput Biol. 2016;12: e1004848. doi:10.1371/journal.pcbi.1004848

22. Wang Y, Rattray JB, Thomas SA, Gurney J, Brown SP. In silico bacteria evolve robust cooperaion via complex quorum-sensing strategies. Sci Rep. 2020;10: 1–10. doi:10.1038/s41598-020-65076-z

23. Goryachev AB. Understanding Bacterial Cell−Cell Communication with Computational Modeling. Chem Rev. 2011;111: 238–250. doi:10.1021/cr100286z

24. James S, Nilsson P, James G, Kjelleberg S, Fagerström T. Luminescence control in the marine bacterium Vibrio fischeri: An analysis of the dynamics of lux regulation. J Mol Biol. 2000;296: 1127–1137. doi:10.1006/jmbi.1999.3484

25. Woltereck. Weitere experimentelle Untersuchungen uber Artveranderung, speziel uber das Wesen quantitativer Artuntershiede bei Daphniden. Science (80-). 1910;32: 344–345. doi:10.1126/science.32.819.344

26. Waddington CH. Canalization of development and the inheritance of acquired characters. Nature. 1942;150: 563–565. doi:10.1038/150563a0

27. Schlichting C, Pigliucci M. Phenotypic Evolution: A Reaction Norm Perspective. 1998.

28. Paaby AB, Testa ND. Developmental Plasticity and Evolution. Evolutionary Developmental Biology. Springer International Publishing; 2018. pp. 1–14. doi:10.1007/978-3-319-33038-9_110-1

29. Scholz RL, Peter Greenberg E. Positive autoregulation of an Acyl- homoserine lactone quorum-sensing circuit synchronizes the population response. MBio. 2017;8. doi:10.1128/MBIO.01079-17

30. Pradhan BB, Chatterjee S. Reversible non-genetic phenotypic heterogeneity in bacterial quorum sensing. Mol Microbiol. 2014;92: 557–569. doi:10.1111/mmi.12575

31. Anetzberger C, Pirch T, Jung K. Heterogeneity in quorum sensing-regulated bioluminescence of *Vibrio harveyi*. Mol Microbiol. 2009;73: 267–277. doi:10.1111/j.1365-2958.2009.06768.x

32. Pérez PD, Hagen SJ. Heterogeneous response to a quorum-sensing signal in the luminescence of individual vibrio fischeri. PLoS One. 2010;5.

453 doi:10.1371/journal.pone.0015473

454 33. Grote J, Krysciak D, Streit WR. Phenotypic heterogeneity, a phenomenon that may
455 explain why quorum sensing does not always result in truly homogenous cell behavior.
456 Applied and Environmental Microbiology. American Society for Microbiology; 2015. pp.
457 5280–5289. doi:10.1128/AEM.00900-15

458 34. Garmyn D, Gal L, Briandet R, Guilbaud M, Lemaître JP, Hartmann A, et al. Evidence of
459 autoinduction heterogeneity via expression of the agr system of Listeria monocytogenes at
460 the single-cell level. Appl Environ Microbiol. 2011;77: 6286–6289.
461 doi:10.1128/AEM.02891-10

462 35. Haseltine EL, Arnold FH. Implications of rewiring bacterial quorum sensing. Appl Environ
463 Microbiol. 2008;74: 437–445. doi:10.1128/AEM.01688-07

464 36. Plener L, Lorenz N, Reiger M, Ramalho T, Gerland U, Jung K. The Phosphorylation Flow
465 of the Vibrio harveyi Quorum-Sensing Cascade Determines Levels of Phenotypic
466 Heterogeneity in the Population. J Bacteriol. 2015;197: 1747. doi:10.1128/JB.02544-14

467 37. PC S, L P, BH I. Activation of the Pseudomonas aeruginosa lasI gene by LasR and the
468 Pseudomonas autoinducer PAI: an autoinduction regulatory hierarchy. J Bacteriol.
469 1995;177: 654–659. doi:10.1128/JB.177.3.654-659.1995

470 38. Papenfort K, Bassler BL. Quorum sensing signal–response systems in Gram-negative
471 bacteria. Nat Rev Microbiol 2016 149. 2016;14: 576–588. doi:10.1038/nrmicro.2016.89

472 39. Dekimpe V, Déziel E. Revisiting the quorum-sensing hierarchy in Pseudomonas
473 aeruginosa: the transcriptional regulator RhlR regulates LasR-specific factors.
474 Microbiology. 2009;155: 712–723. doi:10.1099/MIC.0.022764-0

475 40. Feltner JB, Wolter DJ, Pope CE, Groleau MC, Smalley NE, Greenberg EP, et al. LasR
476 variant cystic fibrosis isolates reveal an adaptable quorum-sensing hierarchy in
477 Pseudomonas aeruginosa. MBio. 2016;7. doi:10.1128/mBio.01513-16

478 41. Almudi I, Vizueta J, Wyatt CDR, de Mendoza A, Marlétaz F, Firbas PN, et al. Genomic
479 adaptations to aquatic and aerial life in mayflies and the origin of insect wings. Nat
480 Commun 2020 111. 2020;11: 1–11. doi:10.1038/s41467-020-16284-8

481 42. Hentzer M, Riedel K, Rasmussen TB, Heydorn A, Andersen JB, Parsek MR, et al.
482 Inhibition of quorum sensing in Pseudomonas aeruginosa biofilm bacteria by a
483 halogenated furanone compound. Microbiology. 2002;148: 87–102.
484 doi:10.1099/00221287-148-1-87

485 43. Burnham KP, Anderson DR, Huyvaert KP. AIC model selection and multimodel inference
486 in behavioral ecology: some background, observations, and comparisons. Behav Ecol
487 Sociobiol 2010 651. 2010;65: 23–35. doi:10.1007/S00265-010-1029-6

488 44. Hartigan JA, Hartigan PM. The Dip Test of Unimodality.
489 https://doi.org/101214/aos/1176346577. 1985;13: 70–84. doi:10.1214/AOS/1176346577

490 45. The evolutionary consequences of plasticity in host–pathogen interactions -
491 ScienceDirect. [cited 10 Nov 2019]. Available:
492 https://www.sciencedirect.com/science/article/pii/S0040580905001644?via%3Dihub

493 46. Via S, Gomulkiewicz R, De Jong G, Scheiner SM, Schlichting CD, Van Tienderen PH.
494 Adaptive phenotypic plasticity: consensus and controversy. Trends in Ecology &
495 Evolution. 1995. pp. 212–217. doi:10.1016/S0169-5347(00)89061-8

496 47. Heilmann S, Krishna S, Kerr B. Why do bacteria regulate public goods by quorum
497 sensing?-How the shapes of cost and benefit functions determine the form of optimal
498 regulation. Front Microbiol. 2015;6. doi:10.3389/fmicb.2015.00767

499 48. Jayakumar P, Thomas SA, Brown SP, Kümmerli R. Pseudomonas aeruginosa reaches
500 collective decisions via transient segregation of quorum sensing activities across cells.
501 bioRxiv. 2021; 2021.03.22.436499. doi:10.1101/2021.03.22.436499

502 49. Darch SE, Simoska O, Fitzpatrick M, Barraza JP, Stevenson KJ, Bonnecaze RT, et al.
503 Spatial determinants of quorum signaling in a Pseudomonas aeruginosa infection model.
504 Proc Natl Acad Sci. 2018;115: 4779–4784. doi:10.1073/PNAS.1719317115

505 50. Fujimoto K, Sawai S. A Design Principle of Group-level Decision Making in Cell
506 Populations. PLOS Comput Biol. 2013;9: e1003110.
507 doi:10.1371/JOURNAL.PCBI.1003110

508 51. Ackermann M. A functional perspective on phenotypic heterogeneity in microorganisms.
509 Nat Rev Microbiol 2015 138. 2015;13: 497–508. doi:10.1038/nrmicro3491

510 52. Cherry JL, Adler FR. How to make a Biological Switch. J Theor Biol. 2000;203: 117–133.
511 doi:10.1006/JTBI.2000.1068

512 53. Schuster M, Urbanowski ML, Greenberg EP. Promoter specificity in Pseudomonas
513 aeruginosa quorum sensing revealed by DNA binding of purified LasR. Proc Natl Acad
514 Sci. 2004;101: 15833–15839. doi:10.1073/PNAS.0407229101

515 54. Ochab-Marcinek A, Tabaka M. Bimodal gene expression in noncooperative regulatory
516 systems. Proc Natl Acad Sci. 2010;107: 22096–22101. doi:10.1073/PNAS.1008965107

517 55. Mellbye B, Schuster M. Physiological framework for the regulation of quorum sensing-
518 dependent public goods in Pseudomonas aeruginosa. J Bacteriol. 2014;196: 1155–1164.
519 doi:10.1128/JB.01223-13

520 56. Diggle SP, Winzer K, Lazdunski A, Williams P, Cámara M. Advancing the quorum in
521 Pseudomonas aeruginosa: MvaT and the regulation of N-acylhomoserine lactone
522 production and virulence gene expression. J Bacteriol. 2002;184: 2576–2586.
523 doi:10.1128/JB.184.10.2576-2586.2002

524 57. Chugani SA, Whiteley M, Lee KM, D'Argenio D, Manoil C, Greenberg EP. QscR, a
525 modulator of quorum-sensing signal synthesis and virulence in Pseudomonas aeruginosa.
526 Proc Natl Acad Sci U S A. 2001;98: 2752–2757. doi:10.1073/pnas.051624298

527 58. Gambello MJ, Iglewski BH. Cloning and characterization of the Pseudomonas aeruginosa
528 lasR gene, a transcriptional activator of elastase expression. J Bacteriol. 1991;173: 3000.
529 doi:10.1128/JB.173.9.3000-3009.1991

530 59. Pearson JP, Passador L, Iglewski BH, Greenberg EP. A second N-acylhomoserine
531 lactone signal produced by Pseudomonas aeruginosa. Proc Natl Acad Sci. 1995;92:
532 1490–1494. doi:10.1073/PNAS.92.5.1490

533 60. Brint JM, Ohman DE. Synthesis of multiple exoproducts in Pseudomonas aeruginosa is
534 under the control of RhlR-RhlI, another set of regulators in strain PAO1 with homology to
535 the autoinducer-responsive LuxR-LuxI family. J Bacteriol. 1995;177: 7155–7163.
536 doi:10.1128/JB.177.24.7155-7163.1995

537 61. Seed P, Passador L, Iglewski BH. Activation of the Pseudomonas aeruginosa lasI gene by
538 LasR and the Pseudomonas autoinducer PAI: an autoinduction regulatory hierarchy. J
539 Bacteriol. 1995;177: 654–659. doi:10.1128/JB.177.3.654-659.1995

62. Casilag F, Lorenz A, Krueger J, Klawonn F, Weiss S, Häussler S. The LasB Elastase of Pseudomonas aeruginosa Acts in Concert with Alkaline Protease AprA To Prevent Flagellin-Mediated Immune Recognition. Infect Immun. 2015;84: 162–171. doi:10.1128/IAI.00939-15

63. Cigana C, Castandet J, Sprynski N, Melessike M, Beyria L, Ranucci S, et al. Pseudomonas aeruginosa Elastase Contributes to the Establishment of Chronic Lung Colonization and Modulates the Immune Response in a Murine Model. Front Microbiol. 2021;0: 3443. doi:10.3389/FMICB.2020.620819

64. Cornforth DM, Dees JL, Ibberson CB, Huse HK, Mathiesen IH, Kirketerp-Møller K, et al. Pseudomonas aeruginosa transcriptome during human infection. Proc Natl Acad Sci. 2018;115: E5125–E5134. doi:10.1073/PNAS.1717525115

65. Winzer K, Williams P. Quorum sensing and the regulation of virulence gene expression in pathogenic bacteria. Int J Med Microbiol. 2001;291: 131–143. doi:10.1078/1438-4221-00110

66. Cox NJ. DIPTEST: Stata module to compute dip statistic to test for unimodality. Stat Softw Components. 2016 [cited 8 Nov 2021]. Available: https://ideas.repec.org/c/boc/bocode/s456998.html

67. Cox NJ, Jenkins SP. GAMMAFIT: Stata module to fit a two-parameter gamma distribution. Stat Softw Components. 2011 [cited 8 Nov 2021]. Available: https://ideas.repec.org/c/boc/bocode/s435301.html

68. Deb P. FMM: Stata module to estimate finite mixture models. Stat Softw Components. 2012 [cited 8 Nov 2021]. Available: https://ideas.repec.org/c/boc/bocode/s456895.html

69. Jann B. PALETTES: Stata module to provide color palettes, symbol palettes, and line pattern palettes. Stat Softw Components. 2020 [cited 8 Nov 2021]. Available: https://ideas.repec.org/c/boc/bocode/s458444.html

70. Jann B. COLRSPACE: Stata module providing a class-based color management system in Mata. Stat Softw Components. 2020 [cited 8 Nov 2021]. Available: https://ideas.repec.org/c/boc/bocode/s458597.html

71. Meisner J, Goldberg JB. The Escherichia coli rhaSR-PrhaBAD inducible promoter system allows tightly controlled gene expression over a wide range in Pseudomonas aeruginosa. Appl Environ Microbiol. 2016;82: 6715–6727. doi:10.1128/AEM.02041-16

72. Winson MK, Swift S, Fish L, Throup JP, JÃ¸rgensen F, Chhabra SR, et al. Construction and analysis of luxCDABE -based plasmid sensors for investigating N -acyl homoserine lactone-mediated quorum sensing . FEMS Microbiol Lett. 1998;163: 185–192. doi:10.1111/j.1574-6968.1998.tb13044.x

73. Fletcher M, Diggle SP, Crusz SA, Chhabra SR, Cámara M, Williams P. A dual biosensor for 2-alkyl-4-quinolone quorum-sensing signal molecules. Environ Microbiol. 2007;9: 2683–2693. doi:10.1111/J.1462-2920.2007.01380.X

74. Hoang TT, Kutchma AJ, Becher A, Schweizer HP. Integration-proficient plasmids for Pseudomonas aeruginosa: site-specific integration and use for engineering of reporter and expression strains. Plasmid. 2000;43: 59–72. doi:10.1006/PLAS.1999.1441

75. Friedman N, Cai L, Xie XS. Linking Stochastic Dynamics to Population Distribution: An Analytical Framework of Gene Expression. Phys Rev Lett. 2006;97: 168302. doi:10.1103/PhysRevLett.97.168302

76. Dempster AP, Laird NM, Rubin DB. Maximum Likelihood from Incomplete Data via the EM Algorithm. J R Stat Soc Ser B. 1977;39: 1–38. Available: http://www.jstor.org/stable/2984875

77. Bailey TL, Elkan C. Fitting a mixture model by expectation maximization to discover motifs in biopolymers. Proceedings Int Conf Intell Syst Mol Biol. 1994;2: 28–36.

78. Abrevaya J, Jiang W. A Nonparametric Approach to Measuring and Testing Curvature. J Bus Econ Stat. 2005;23: 1–19. Available: http://www.jstor.org/stable/27638790

Supplementary Information for *Bacterial quorum sensing allows graded and bimodal cellular responses to variations in population density*

Jennifer B. Rattray[1,2], Stephen A. Thomas[1,2,3], Yifei Wang[1,2,4], Evgeniya Molotkova[1], James Gurney[1,2], John J. Varga[1,2], Sam P. Brown[1,2]

[1] School of Biological Sciences, Georgia Institute of Technology, Atlanta, 30332 GA, USA
[2] Center for Microbial Dynamics and Infection, Georgia Institute of Technology, Atlanta, 30332 GA, USA
[3] Graduate Program in Quantitative Biosciences (QBioS), Georgia Institute of Technology, Atlanta, 30332 GA, USA
[4] The Institute for Data Engineering and Science (IDEaS), Georgia Institute of Technology, Atlanta, 30332 GA, USA

Corresponding author: Sam P. Brown

Email: sam.brown@biology.gatech.edu

Data Supplement

- **Figure S1.** Growth curves across different carbon limiting environments
- **Figure S2.** Microplate population per capita data is graded and linear
- **Figure S3.** Ridgeline density plot of all single cell *lasB* reporter response data
- **Figure S4.** Hartigan's Dip Test Statistic
- **Figure S5.** Single cell results are not sensitive to the exact time sampled
- **Figure S6.** Presence/absence of *Plac::lasR* and plasmid nature of the reporter do not impact graded QS response
- **Figure S7.** Population response to density using chromosomal lux-based QS reporters
- **Figure S8.** Visual summary of single-cell microscopy analysis pipeline
- **Table S1.** Strains used in this manuscript

Analysis Supplement

- **Figure S9.** Comparison of pixel intensity distribution for Δ*lasI*Δ*rhlI* and wildtype strains
- **Figure S10.** Two-component Gamma mixture model of expression level distributions overlaid on observation histograms
- **Figure S11.** Comparing model predictions with observations for optical density values that demonstration statistically significant bimodality
- **Figure S12.** Comparing model predictions at moderate optical densities
- **Figure S13.** Comparing a model of a single Gamma distribution to the two-component mixture
- **Table S2.** Information criteria for single Gamma and two-component Gamma mixture models at low optical densities

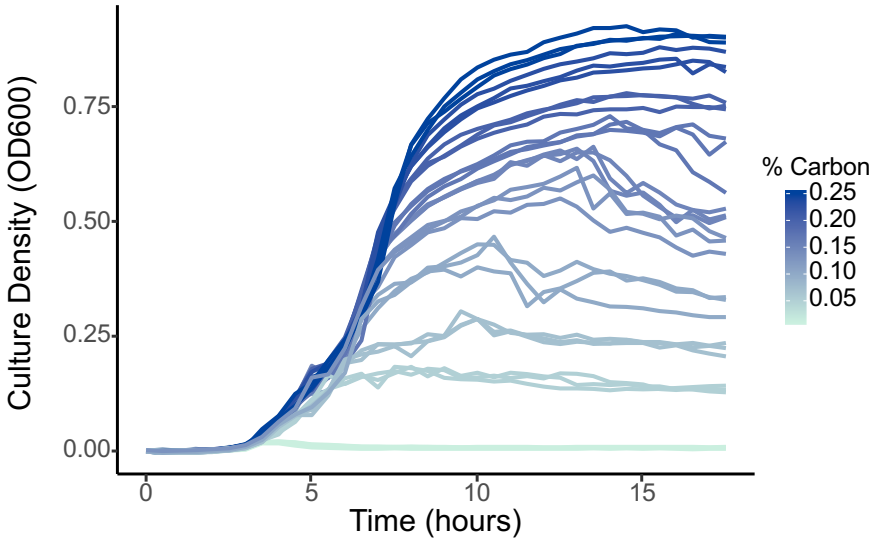

Figure S1. Growth curves for PAO1 pMHLAS across different carbon limiting environments. Discrete environmental densities can be generated by varying carbon availability, therefore manipulating the carrying capacity of the culture.

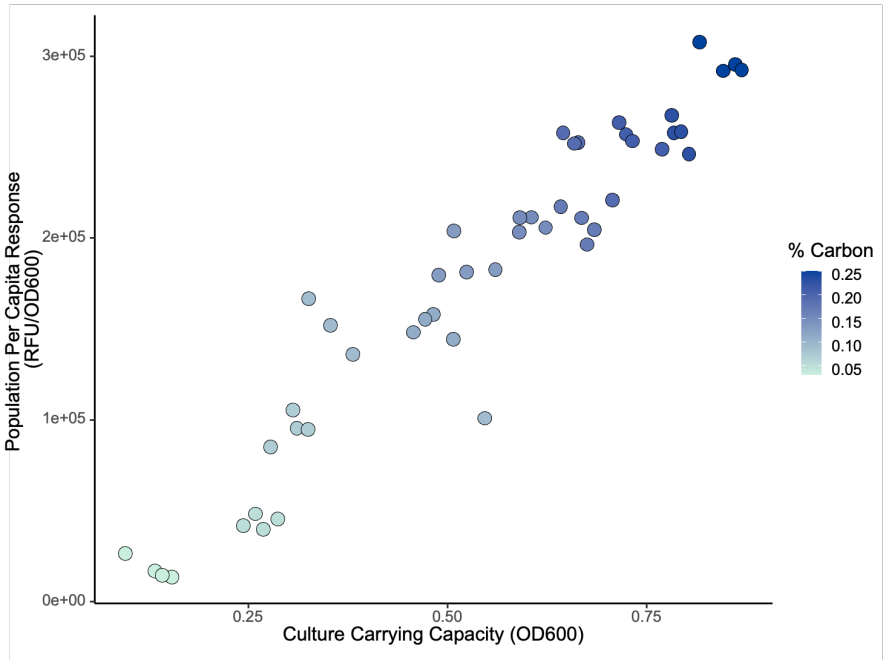

Figure S2. Microplate population per capita data is graded and linear. PAO1 pMHLAS was grown as mentioned in the methods and fluorescence and OD_{600} were measured on a Cytation Sense plate reader. Microplate results agree with microscopy results that that population response to increasing cell density is linear and graded. OD_{600} of 0.25 is 5.5×10^8 cells/ml, OD_{600} of 0.50 is 1.3×10^9 cells/ml, and OD_{600} of 0.75 is 2.05×10^9 cells/ml.

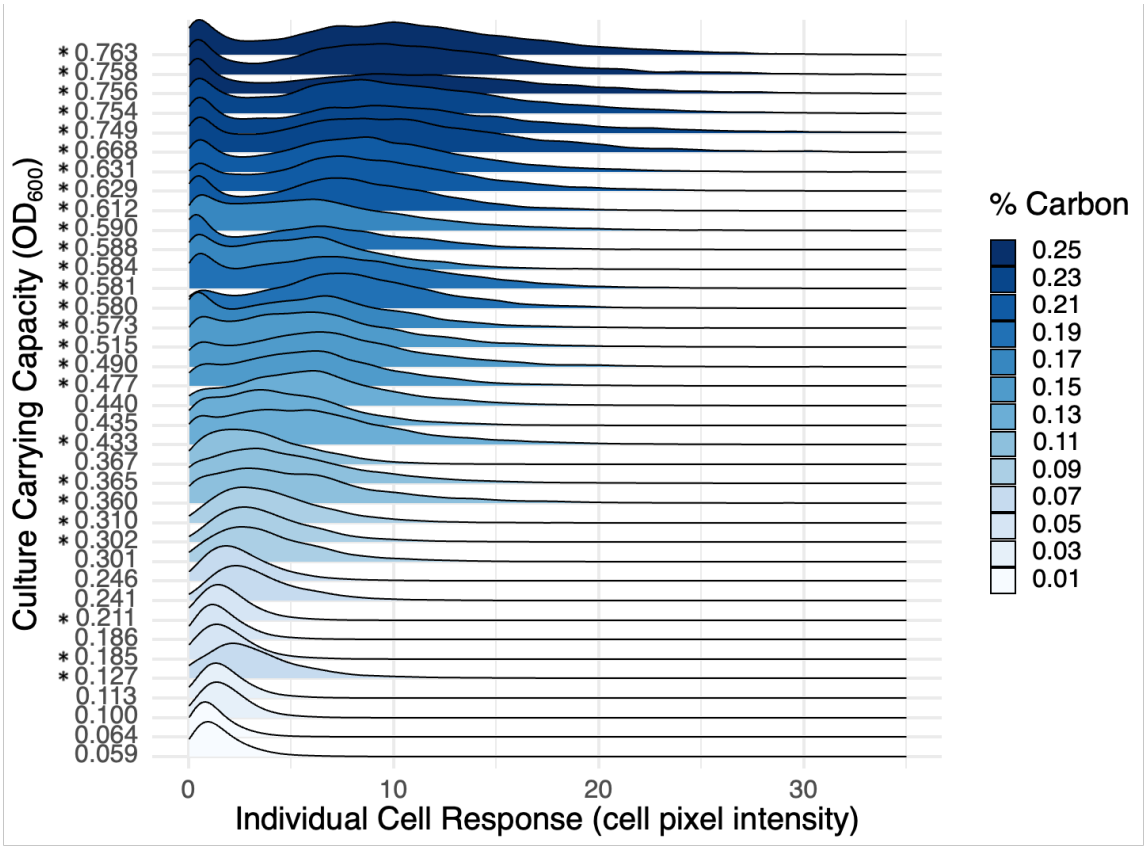

Figure S3. Ridgeline density plot (bandwidth = 0.529) of single-cell *lasB* reporter response data showing the distribution of individual cell QS expression across the population. All 39 replicates are plotted separately. Asterisks indicate significant bimodality (Hartingan's Dip Test [44], Figure S4).

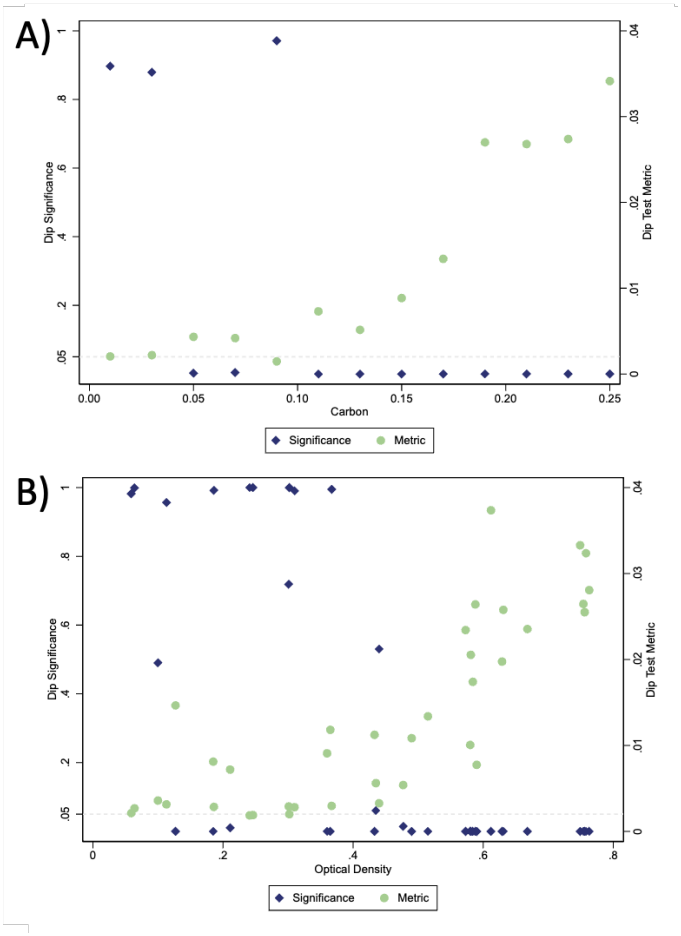

Figure S4. Hartigan's Dip Test. A) Results of Hartigan's dip test [44] for assessing bimodality of the expression level distributions at each carbon level for data shown in Figure 4. B) Results of Hartigan's dip test for assessing bimodality of the expression level distributions at each OD level for data shown in Figure S3. Statistical significance in the form of p-value is plotted in yellow on the left axis, and the dip metric is plotted in green on the right axis. The most conservative p-value is shown.

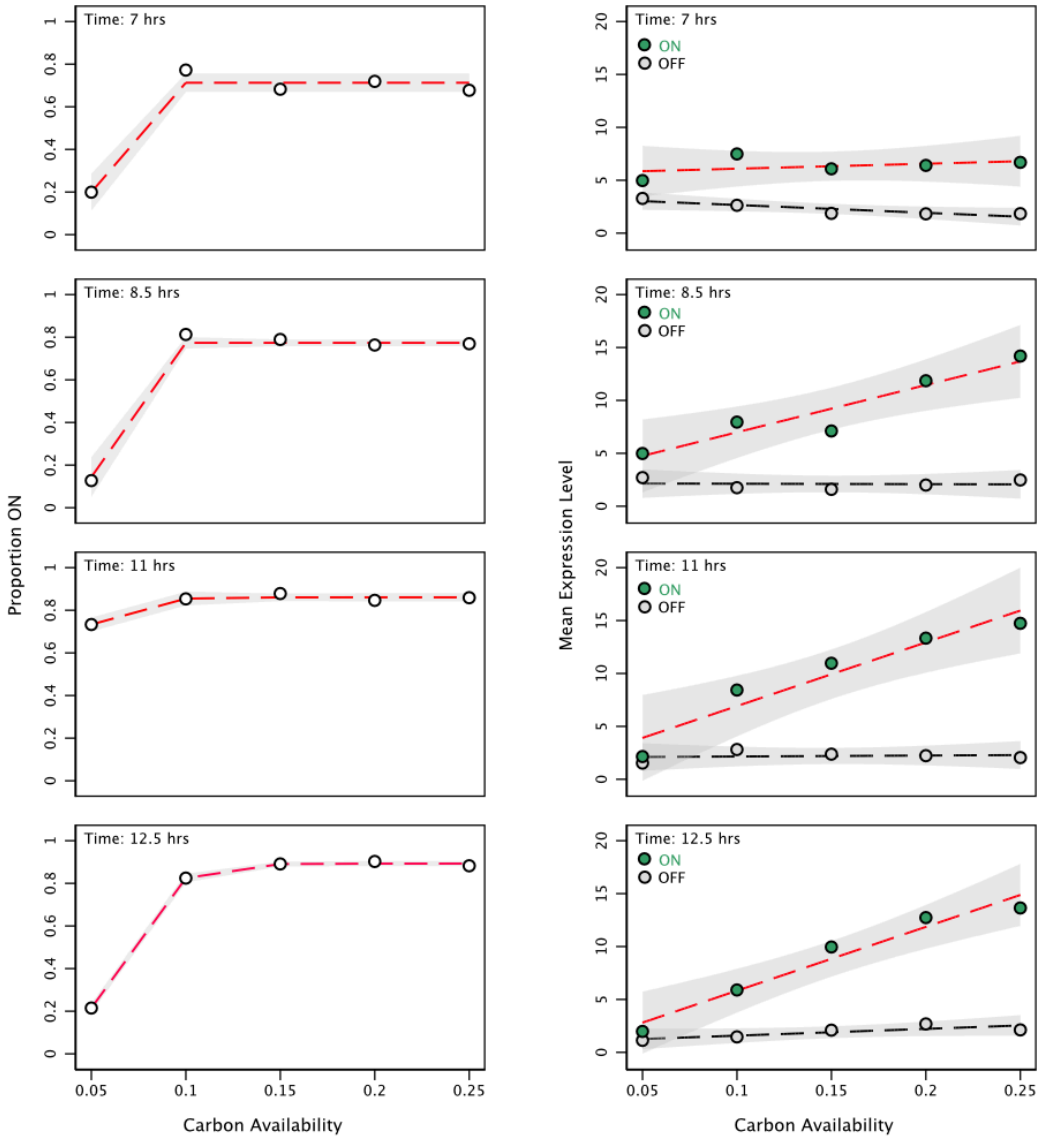

Figure S5. Single cell results are not sensitive to the exact time sampled. In order to test the generality of our results and how sensitive they are to the specific time sampled, we repeated our main experiment with PAO1 pMHLAS, but took samples from five different time points instead of just entry into stationary phase. We observed the same bimodal response and shifts in proportion responding and level of response across all timepoints, concluding that our results are not sensitive to the exact measurement time.

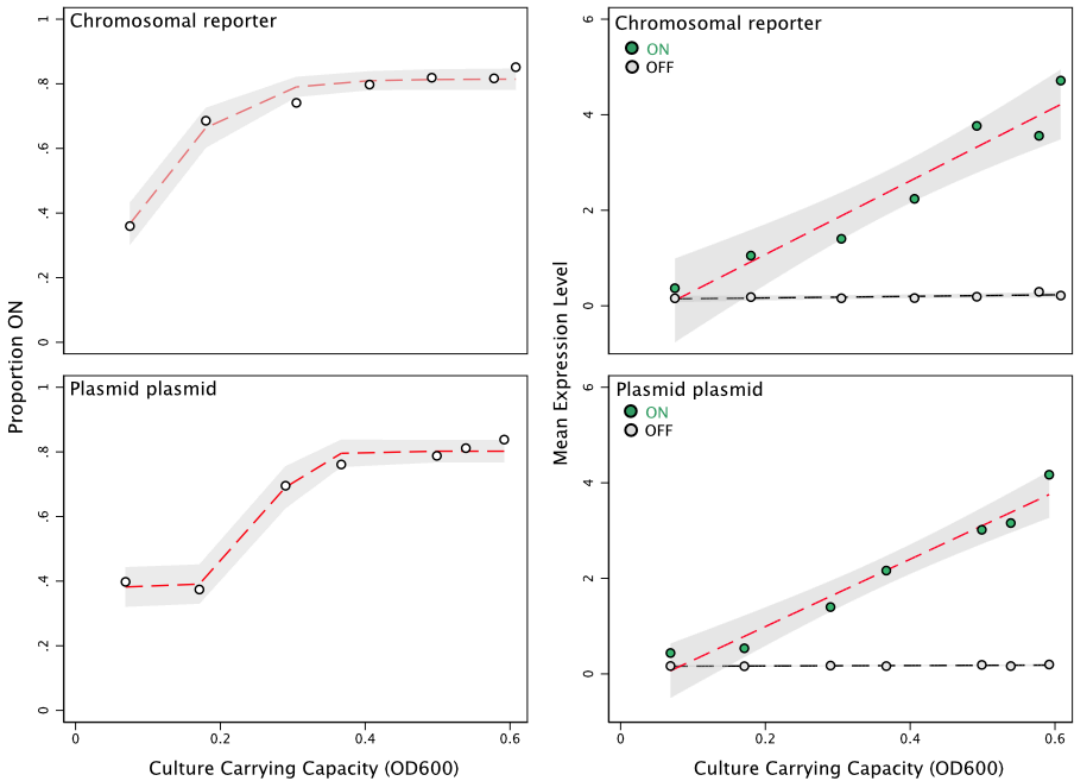

652

653 **Figure S6. Presence/absence of *Plac::lasR* and plasmid nature of the reporter do not impact graded**
654 **QS response.** The plasmid hosting our reporter, pMHLAS, also contains P*lac::lasR.* While the lac operon is
655 typically repressed, some strains of *Pseudomonas* are capable of leaky, non-induced expression [71]. To
656 confirm our single cell data, we repeated the experiment using a strain with the P*lasB::gfp(ASV)* reporter
657 inserted with the mini-Tn5 method. This strain does not contain P*lac::lasR* and expresses WT levels of *lasR*.
658 We found the same bimodal response to density environments in both strains. This indicates that neither the
659 presence of P*lac::lasR* nor the plasmid-based nature of our reporter are responsible for the graded QS
660 response. This could mean either there is not an appreciable amount of *lasR* being made from the
661 P*lac::lasR* or that the increase of *lasR* does not impact the observed response. These results confirm that
662 the observed response across density is not sensitive to plasmid copy number or the presence of potentially
663 leaky P*lac::lasR* with this specific reporter.

664

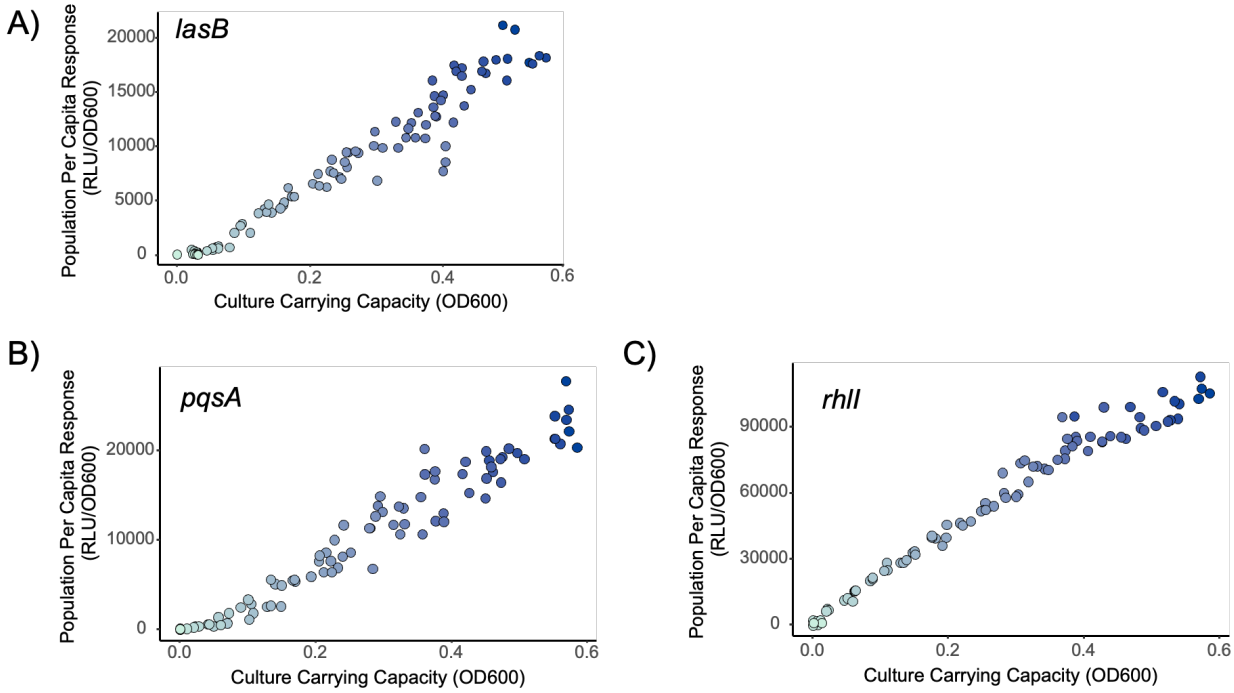

Figure S7. Population response to increasing cell density using chromosomally inserted lux based QS reporters. A) strain P NPAO1 mini-CTX PlasB::lux, B) NPAO1 mini-CTX PpqsA::lux, and C) NPAO1 mini-CTX PrhlI::lux. Bacteria were grown following the same methods outlined in the main text methods and monitored in a plate reader. Per capita expression (RLU/OD_{600}) was calculated by taking the maximum expression (RLU) divided by the carrying capacity of the culture (OD_{600}). With all three QS reporters, a linear fit model supports the data more than a step-function fit (lasB, AIC linear: 0, AIC step-function: 281.55. pqsA, AIC linear: 1.22, AIC step-function: 283.43. rhlI, AIC linear: 40.68, AIC step-function: 351.86).

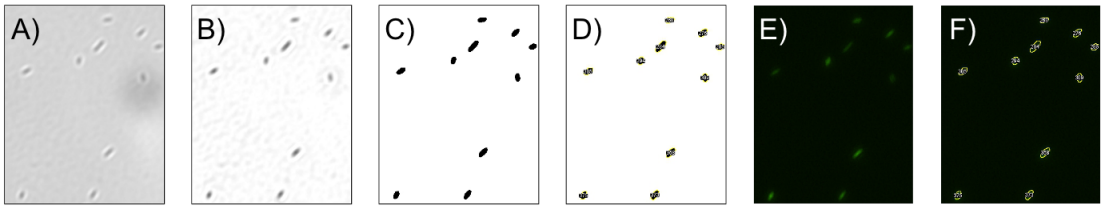

Figure S8. Visual summary of single-cell microscopy analysis pipeline. A) Phase contrast image of individual cells immobilized on 0.01% poly-l-lysine coated glass slides. B) ImageJ's "background subtraction" command was used to increase contrast between the cells and the background. C) A mask of the phase contrast channel was then created using ImageJ's default auto threshold, a variation of the IsoData algorithm. D) ImageJ's "analyze particles" command was then used to identify the features (cells) from the image, this generates a set of regions of interest (ROIs), shown in yellow superimposed. E) Unaltered fluorescence channel image of the same cells. F) ROIs generated from the phase contrast image are then be superimposed onto the unedited fluorescence channel image, either red fluorescence for dead cell identification via propidium iodide or green florescence for the QS reporter, and ImageJ's "measure" command was used to find the average pixel intensity within each ROI. Any ROIs with red fluorescence were identified as compromised cells and removed from further analysis.

Strain/Plasmid	Relevant Characteristics	Figure	Source or Reference
NPAO1 pMHLAS	QS reporter *PlasB::gfp(ASV), Plac::lasR*	2, 3, 4, S1, S2, S4, S5	Hentzer et al., 2002 [42]
NPAO1 *ΔlasIΔrhlI* pMHLAS	Double signal synthase mutant, QS reporter *PlasB::gfp(ASV)*	2, 3, 4	This paper
PAO1 MH340 mini-Tn5 *PlasB::gfp(ASV)*	QS reporter *PlasB::gfp(ASV)* inserted via the mini-Tn5 method	S5	Kasper Nørskov Kragh
NPAO1 mini-CTX P*lasB::lux*	luxCDABE based [72] QS reporter [73] inserted at the *attB* site [74]	S6	This paper
NPAO1 mini-CTX P*pqsA::lux*	luxCDABE based [72] QS reporter [73] inserted at the *attB* site [74]	S6	This paper
NPAO1 mini-CTX P*rhlI::lux*	luxCDABE based [72] QS reporter [73] inserted at the *attB* site [74]	S6	This paper

687 **Table S1. Strains used in this manuscript.**

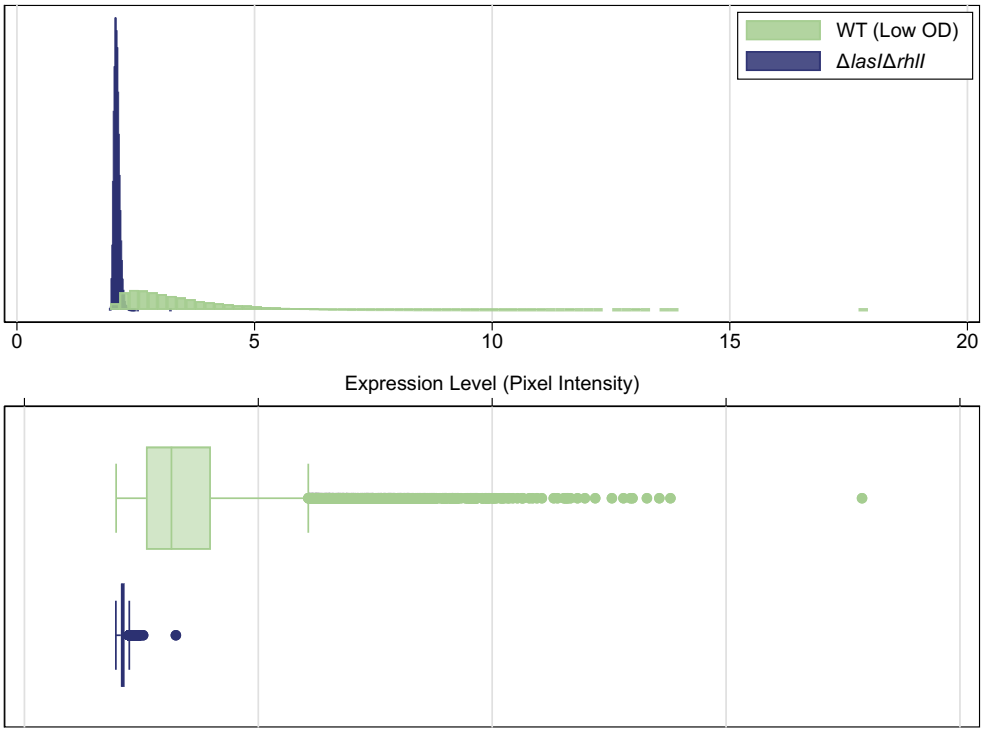

Figure S9. Comparison of pixel intensity distribution for Δ*lasI*Δ*rhlI* and wildtype strains. Figure S1 shows the observed pixel intensity measurements for Δ*lasI*Δ*rhlI* cells in comparison to those for wildtype cells at the lowest measured optical density (OD). As the Δ*lasI*Δ*rhlI* strain is incapable of synthesizing auto-inducers, it should exhibit minimal *lasB* expression. The standard deviation is for expression in the wildtype is1.23. In contrast, pixel intensity for the Δ*lasI*Δ*rhlI* strain is confined to a very narrow range; its standard deviation is 0.06. These results are consistent with a mutant strain that does not express *lasB* suggesting that the mutant's pixel intensity is near the measurement sensitivity of the experiment. Indeed, the minimum pixel intensity observed in the mutant is 1.955, a value consistent with the overall minimum observed intensity of 1.952. Treating this value as the measurement limit, we subtract it from all measured intensities so that an intensity of 0 corresponds to no expression. The main text figures use *adjusted expression level* to indicate the measured pixel intensity after subtracting this minimum value.

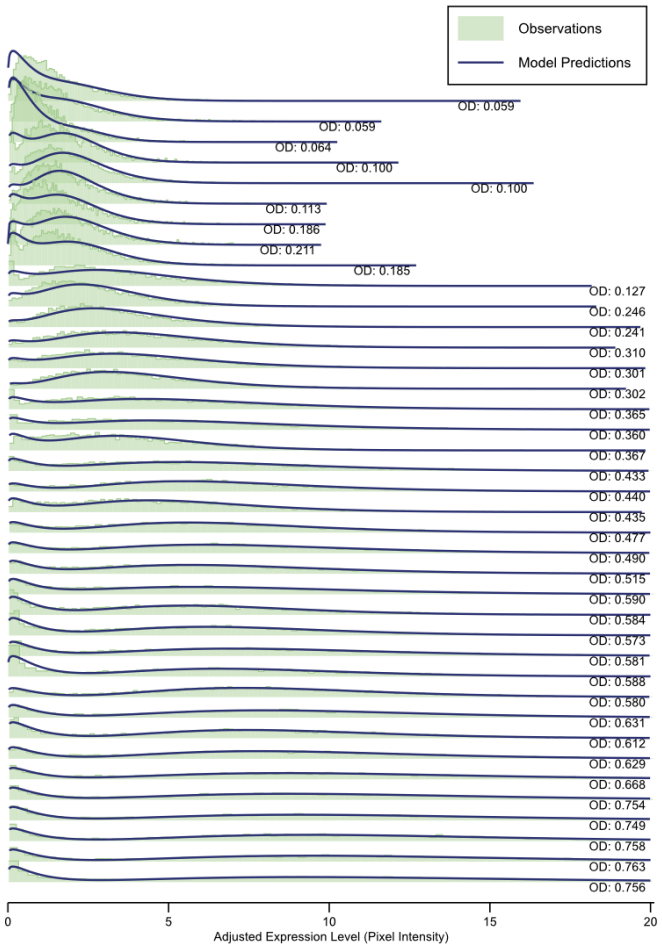

Figure S10. Two-component Gamma mixture model of expression level distributions overlaid on observation histograms. After having identified two sub-populations of cells (Figure S3, Figure S4) we model the observed *lasB* expression levels as a two-component finite mixture model. The sub-populations serve as a latent classes in the model. As gene expression level is non-negative and necessarily right-skewed, we use the Gamma distribution to model expression levels of each class [75,76]. We use expectation-maximization [77,78] to find maximum likelihood estimates for the latent class probabilities and Gamma distribution parameters at each density. Our initial model places no constraints on the parameters other than those required by the model structure (i.e. probabilities between 0 and 1, shape and scale positive). Three parameters from the mixture model characterize the sub-populations of cells: the proportion of cells in the ON sub-population and the mean *lasB* expression levels of the ON and OFF sub-populations. To improve the model's discriminatory power at low densities, we constrain the OFF sub-population parameters to be those values from the higher densities and update the estimates solely for the ON sub-population. The highest optical density values demonstrate statistically significant bimodality. As expected, the mixture model accurately captures the two sub-populations that make up these distributions. Figure S11 compares these models with the observations.

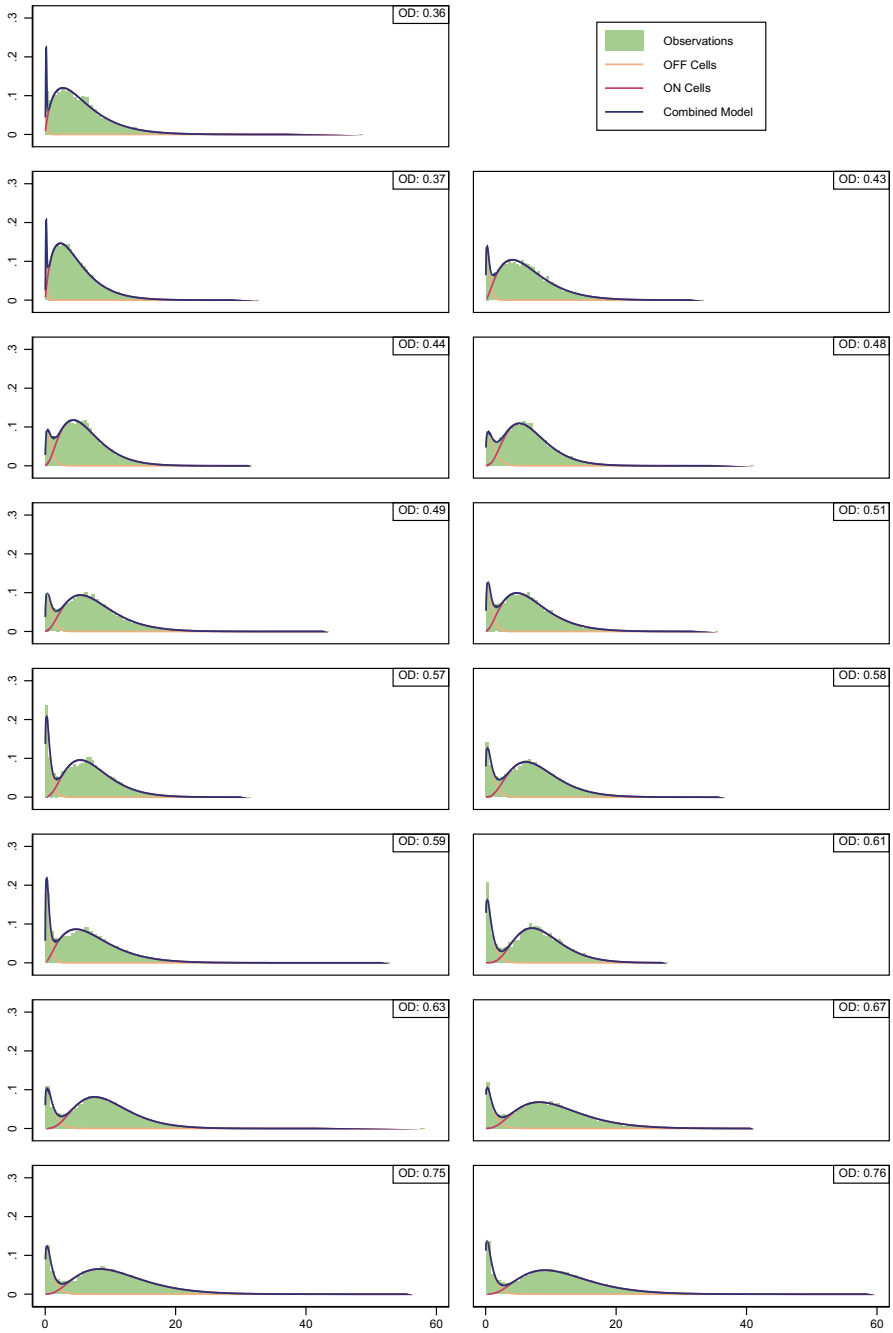

Figure S11. Comparing model predictions with observations for optical density values that demonstration statistically significant bimodality. In addition to the complete model (shown in blue), the plots also show the individual sub-populations of OFF cells (yellow) and ON cells (red). At medium optical density values, the mixture model predictions continue to show close agreement with the observations. Figure S12 highlights this agreement. OD values that don't demonstrate statistically significant bimodality still show the effects of a mixture of two sub-populations.

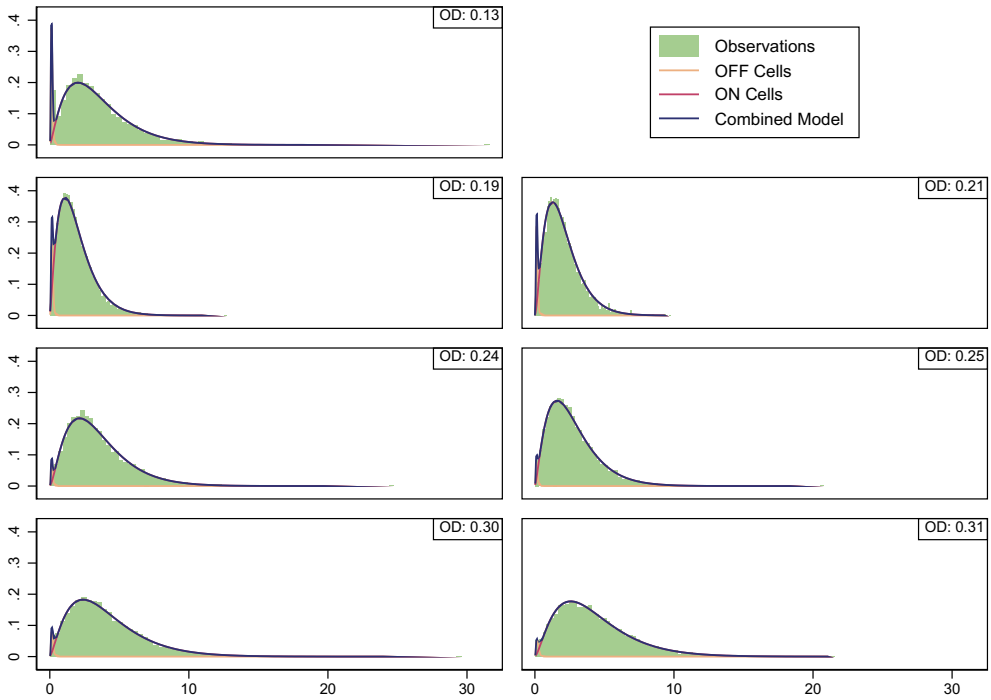

Figure S12. Comparing model predictions at moderate optical densities. As above, the plots show the individual sub-populations of OFF cells (yellow) and ON cells (red). At the lowest optical densities, the benefits of a mixture model are less clear. Figure S13 illustrates the difficulty by comparing the mixture model with a maximum likelihood fit to a single Gamma distribution. As Table S2 indicates, both Akaike Information Criteria (AIC) and Bayesian Information Criteria (BIC) suggest that the mixture model is superior, but the visual evidence is less compelling.

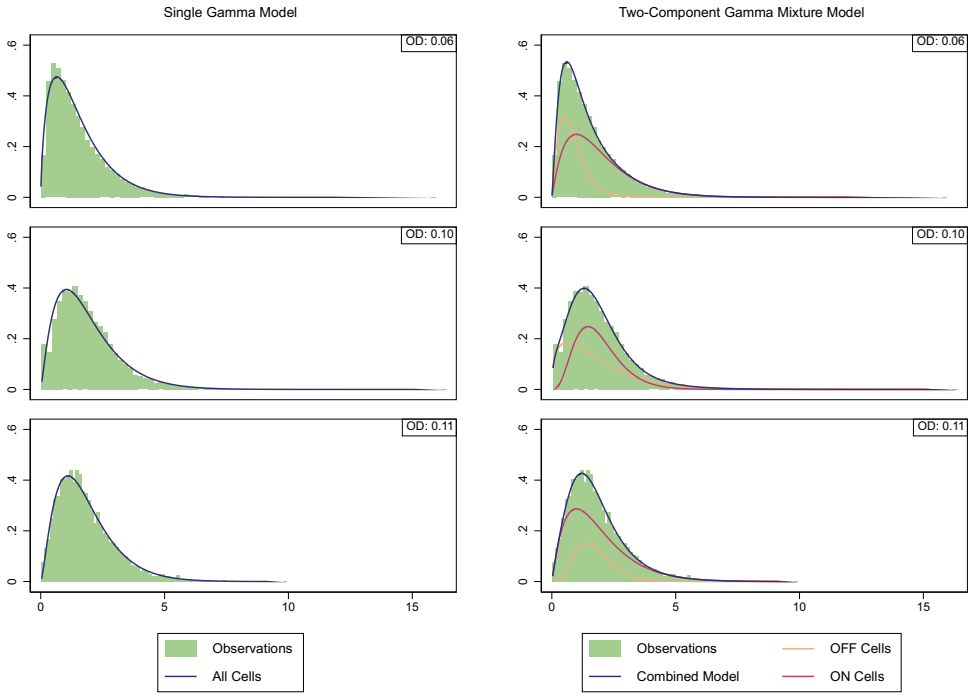

732

733 **Figure S13. Comparing a model of a single Gamma distribution to the two-component mixture.** Plots
734 on the right show a single Gamma distribution with maximum likelihood estimates for shape and scale
735 parameters. Plots on the right show the two-component mixture model. Mixture model plots include
736 individual sub-populations of OFF cells (yellow) and ON cells (red). As the figure and table both show, the
737 observations at optical density 0.11 are especially problematic. At that OD, the statistical mode of *lasB*
738 expression in the ON sub-population is lower than that in the OFF sub-population. As required by the model,
739 however, the mean expression level of the ON sub-population is higher than that of the OFF sub-population.

740

OD	AIC_1	AIC_2	ΔAIC	BIC_1	BIC_2	ΔBIC	LR $\chi^2(3)$	p-value
0.06	55741	55472	-268	55757	55512	-245	274	0
0.10	33499	33289	-210	33514	33326	-188	216	0
0.11	20994	20972	-22	21008	21007	-1	28	3.5×10^{-6}

Table S2. Information criteria for single Gamma (subscript 1) and two-component Gamma mixture (subscript 2) models at low optical densities. The Δ columns show change in associated information criteria in two-component model. Final two columns are likelihood ratio and p-value.